

Sensitivity analysis of geometrical parameters to study haemodynamics and thrombus formation in the left atrial appendage

Guadalupe Garcia-Isla¹, Andy L. Olivares¹, Etelvino Silva², Marta Nuñez-Garcia¹, Constantine Butakoff¹, Damian Sanchez-Quintana³, Hernan G. Morales^{4,5}, Xavier Freixa⁶, Jerome Noailly¹, Tom de Potter², Oscar Camara¹

¹DTIC, Department of Information and Communication Technologies, Universitat Pompeu Fabra, Barcelona, Spain

²Arrhythmia Unit, Department of Cardiology, Cardiovascular Center, Aalst, Belgium

³Department of Anatomy, University of Extremadura, Badajoz, Spain

⁴Medisys, Philips Research, Paris, France

⁵Centro de Fisiologia del Ejercicio, Facultad de Ciencias, Universidad Mayor, Santiago de Chile, Chile

⁶Department of Cardiology, Hospital Clinic de Barcelona, Universitat de Barcelona, Barcelona, Spain

SUMMARY

The left atrial appendage (LAA) is a complex and heterogeneous protruding structure of the left atrium (LA). In atrial fibrillation (AF) patients, it is the location where 90% of the thrombi are formed. However, the role of the LAA in thrombus formation is not fully known yet. The main goal of this work is to perform a sensitivity analysis to identify the most relevant LA and LAA morphological parameters in atrial blood flow dynamics. Simulations were run on synthetic ellipsoidal left atria models where different parameters were individually studied: pulmonary veins (PV) and mitral valve (MV) dimensions; LAA shape; and LA volume. Our computational analysis confirmed the relation between large LAA ostia with low blood flow velocities and thrombus formation. Additionally, we found PV configuration exerted a critical influence on LAA blood flow patterns. These findings contribute to a better understanding of the LAA structure and to the support of clinical decisions for AF patients.

Received ...

KEY WORDS: Computational Fluid Dynamics, blood flow patterns, morphology, left atrial appendage, sensitivity analysis, thrombus formation, medical images

*Correspondence to: *Oscar Camara PhD, DTIC, C/Tanger,122-140, 08018, Barcelona Spain. oscar.camara@upf.edu

This article has been accepted for publication and undergone full peer review but has not been through the copyediting, typesetting, pagination and proofreading process, which may lead to differences between this version and the Version of Record. Please cite this article as Int. J. Numer. Meth. Biomed. Engng., e03100. doi: 10.1002/cnm.3100

1. INTRODUCTION

Around 70-90% of thrombi in non-valvular atrial fibrillation (AF) patients are formed in the left atrial appendage (LAA), a protruding structure located in the left atrium [18, 30]. The LAA is known to act as a decompression chamber during left ventricular systole and in periods of high left atrial pressure [2]. Chronic atrial fibrillation (AF) causes rigidity on LA walls, preventing its proper contraction [28]. Likewise, this condition alters normal left atrial haemodynamics and leads to blood stagnation in the LAA, increasing the risk of thrombus formation [8, 5].

The most deleterious consequence regarding thrombus formation is the possibility of its dislodging and liberation onto the circulatory system, as it may travel to the brain and cause an embolic stroke. Oral anticoagulant treatments are initially considered for reducing the risk of thrombus formation [27, 34]. Differently, the high number of patients with contraindications to anticoagulant therapies, mainly due to high haemorrhagic risk, are subjected to a LAA physical isolation [25]. The devices used for LAA closure have to cope with the highly heterogeneous structural nature of the appendages for fulfilling their occluding function [16, 10]. However, due to the LAA morphological heterogeneity and the difficulty in acquiring LA haemodynamics data, the LAA role and importance in LA functionality remains uncertain. Therefore, the consequences of its occlusion are not fully understood and controlled, which may lead to possible unknown physiological sequelae.

Left atrial appendages are characterized by a high patient-specific geometrical variability [13, 4]. Using necropsy synthetic resin cast, Ernst et al. [7] analyzed 220 LAA morphologies and reported variations of: LAA volume between 0.7 – 19.2 mL; for maximum ostium diameter between 10 – 40 mm; and length ranging from 16 – 51 mm. Advanced imaging techniques such as Computational Tomography (CT) or 3D Rotational Angiography (3DRA) provide accurate 3D reconstructions of LAA geometries. Researchers have proposed to classify them into four different types of shapes [5]: chicken wing, windsock, cactus or cauliflower. It was recently reported that patients with non-chicken wing LAA morphology were more prone to undergo thromboembolic events than those with chicken wing LAA type [18, 5]. However, this morphological classification is based on indices that are not always well defined and reproducible such as the notion of dominant/secondary lobes or structural complexity; in consequence it is often difficult to reach a consensus about the different categories. Furthermore, relevant structural information around the LAA such as pulmonary vein configuration and LA volume are never considered. Therefore, the relationship between LAA morphology and stroke is still controversial.

The influence of LAA haemodynamics on thrombus formation has been studied by many researchers [5, 21, 3]. The main factors causing thromboembolic events are described by Virchow's triad [28]: hypercoagulability, haemodynamic changes, and endothelial injury dysfunction. Therefore, a decrease in fluid velocity within the LAA is directly related to an increased risk of thrombus formation. Blood flow information is usually measured from Transesophageal Echocardiographic (TEE) images (including Doppler acquisitions) before and after LAA occlusion interventions to plan and evaluate the correct positioning of the device. However, they only provide partial flow data on a plane or a given point of view. Several studies [3, 8, 11] suggest that among patients with AF, subgroups with low LAA flow velocities are associated with a higher risk of stroke and the presence of spontaneous echocardiographic contrast (< 0.4 m/s) and even with the identification of thrombus within the LAA and a higher incidence of thromboembolic events (< 0.2 m/s). Nevertheless, this velocity-based parameter, measured in one point in space (LAA ostium) and time (end diastole), constitutes a non-reproducible and too simple index for characterizing the complex patterns of LAA haemodynamics. Detailed haemodynamic characterization is nowadays possible using the novel 4D-flow Magnetic Resonance Imaging (MRI) technique [19, 6], yet it is still in its infancy.

Computational modelling approaches simulating the physical and biological behavior of physiological organs have been developed to comprehensively analyze blood flow characteristics and predict thrombus formation in other regions of the human body. For instance, a 3D computational fluid dynamic (CFD) study on abdominal aortic aneurisms [1] suggested that shear flow, spatially and temporally determined, influenced endothelium activation, thus promoting thrombus formation. A few number of papers [33, 29, 14, 24] can be found in literature with CFD studies of LA/LAA configurations performed merely on synthetic geometries or in 1-2 patient-specific geometries acquired with CT/MR imaging, but without jointly analyzing haemodynamic and morphological indices to investigate the risk of thrombus formation. In previous preliminary studies [23, 22] based on CFD simulations run on patient-specific LAA geometries, we found that non-chicken-wing LAA morphologies were associated to indices linked to higher risk of thrombus formation (e.g. flow vortices). In addition, the obtained results suggested the importance of analyzing the whole atrial configuration (i.e. PV patterns, LA volume) together with different LAA morphologies. However, the comparison among haemodynamics of different patient-specific LA/LAA geometries is hampered by the great amount of varying morphological parameters describing each geometry and influencing atrial blood flow. The aim of the present paper is to perform a sensitivity analysis to assess the specific contribution of several morphological descriptors in the haemodynamics of different artificially generated LA/LAA configurations and their potential relation with thromboembolic events. The combined analysis of morphological descriptors with

haemodynamics could shed light on the relevance of the LAA structure and its role in the cardiovascular system.

2. MATERIALS AND METHODS

Patient-specific LA data was used as baseline for the design and creation of a sensitivity analysis where several synthetic left atria were generated for the study of the influence of: PVs and MV dimensions; LA volume; and LAA structure. The final synthetic dataset was composed of 36 different LA/LAA configurations. LA tetrahedral meshes were built with a modelling pipeline using several Open-Source software: Gmsh [†], Autodesk MeshMixer [‡] and MeshLab [§]. CFD simulations over one cardiac cycle were obtained with the ANSYS Fluent (Academic Research CFD version) solver. Post-processing of the CFD simulations results initially derived the following indices to characterize blood flow patterns at each time step: Reynold number, pressure values, velocity vectors (in different regions such as the mitral valve = MV, and the LAA), vorticity, wall shear stress (WSS) and shear strain magnitudes. These parameters were posteriorly visualized with ParaView [¶] (5.2.0-RC3 version) for their further analysis and manipulation, including blood flow streamlines and vorticity patterns. Additionally, more advanced haemodynamics descriptors related to thrombus formation were estimated (using Matlab R2016b; The Mathworks, MS, USA) such as the time-averaged WSS (TAWSS), the oscillatory shear index (OSI), the relative residence time (RTT) and the endothelial cell activation potential (ECAP). All these haemodynamics descriptors were integrated regionally for the LAA and the rest of the LAA independently. The 90th percentile of these parameter values were taken for their posterior statistical analysis and comparison in the designed experiments to evaluate the significance of each morphological descriptor under study.

2.1. Left atrial appendage meshes from imaging data

Patient-specific data was used as the starting point of the simulation pipeline (see Figure 1). Eleven patients with paroxysmal atrial fibrillation from the OLV Hospital in Aalst, Belgium, were selected for our study. The local ethical committee approved this study and informed consent was obtained from every participant. All patients presented a low risk of thrombus formation according to the clinically used CHADSVASC score (equal to zero or 1). 3D Rotational Angiography (3DRA) images were acquired with an Innova 3D system (GE Healthcare, Chalfont St Giles, UK) and

[†]<http://gmsh.info/>

[‡]<http://www.meshmixer.com/>

[§]<http://www.meshlab.net/>

[¶]<https://www.paraview.org/>

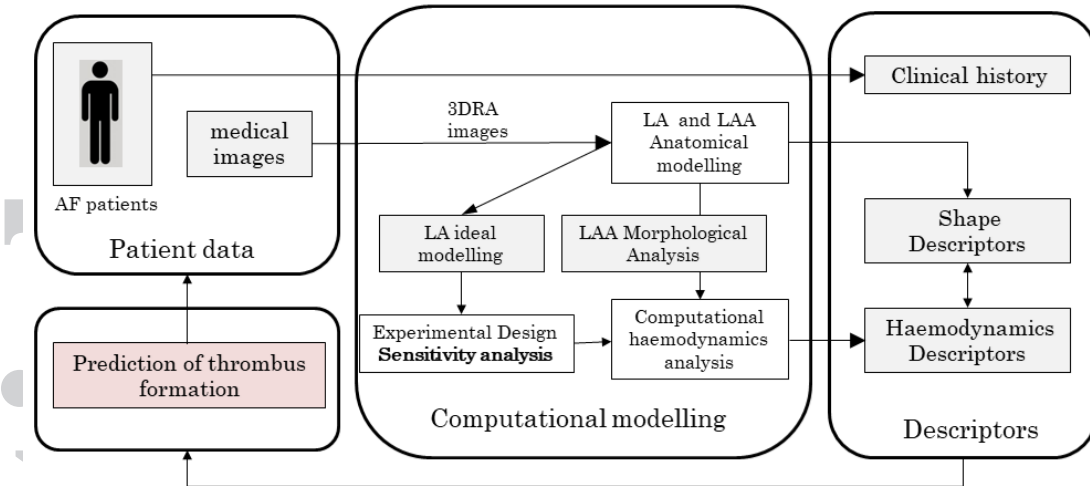


Figure 1. Data processing for evaluation of LA and LAA morphologies and its haemodynamics descriptors to predict the thrombus formation. The sensitive study focused on LAA morphologies and some parameters of the ideal LA used in the creation different synthetic patient models.

Table I. Population-based statistics from imaging data guiding the generation of synthetic left atria (LA) configurations. LAV: LA volume; PVs: pulmonary veins; MV: mitral valve. Levels and magnitude: low (L), average (A) and high (H).

| Parameters | Levels and magnitude | | | Combinations of Levels | | | | | | | | |
|------------------------|----------------------|---------|----------|------------------------|----|----|----|----|----|----|----|----|
| | Low (L) | Avg (A) | High (H) | LL | LA | LH | AL | AA | AH | HL | HA | HH |
| LAV (mL) | 121.1 | 170.6 | 250.2 | L | L | L | A | A | A | H | H | H |
| PVs (cm ²) | 1.22 | 1.95 | 3.05 | L | A | H | L | A | H | L | A | H |
| MV (cm ²) | 6.03 | 8.56 | 12.50 | L | A | H | L | A | H | L | A | H |

reconstructed with the scanner workstation, providing isotropic 3D images with 0.23 mm and 0.45 mm volumetric pixel size for 512 and 256 pixels per dimension, respectively. Segmentation of LA/LAA was achieved with semi-automatic thresholding and region-growing algorithms available at the scanner console. From the resulting binary masks, surface triangular-element meshes were generated with the classical Marching Cubes method. A Taubin filter was applied (using Meshlab) for smoothing the surface meshes while preserving the original volume.

2.2. Synthetic model of the left atria

From the study of the AF patient database we obtained atrial volumes and dimensions for their PVs and MV. Using these measurements, we estimated their basic statistics using the maximum, average and minimum population trends, obtaining three different levels for each variable. These values were used for the creation of three synthetic ellipsoidal left atria, where PV and MV were manually incorporated (using Meshmixer) following the spatial locations of a real LA case as a template (Figure 2a). Combining these elements, we built a set of nine different LA configurations (see Table I) that consistently enabled the analysis of their individual contribution to the overall model. Out of the eleven patients, four different LAAs representing their large geometrical variability were

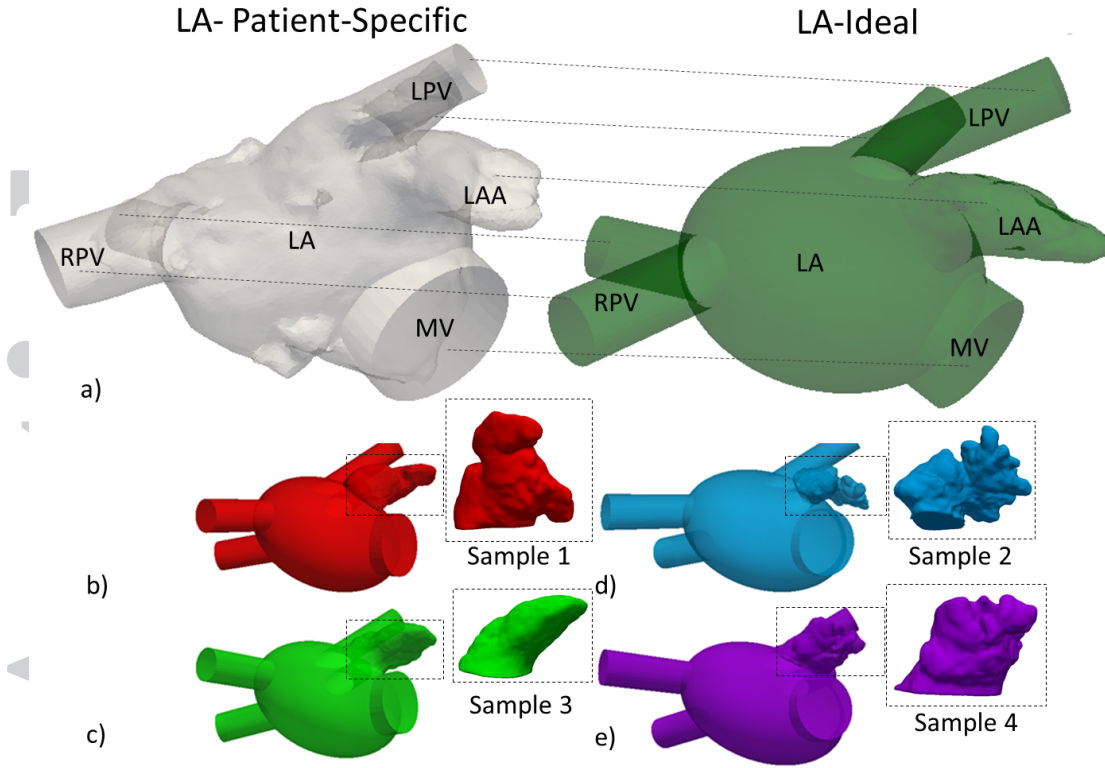


Figure 2. a) Patient-specific model used as a reference to create the synthetic left atria (LA) model. the ideal one including a realistic left atrial appendage (LAA). b-e) Synthetic LA integrated with four different patient-specific LAA geometries.

chosen (Figure 2b-e). These appendages were placed and integrated into the synthetic ellipsoidal LA models respecting the spatial relationships with respect to the PV and MV of the real LA template. These configurations yielded 36 different LA/LAA synthetic models (see Table I), where in each one of them only one morphological parameter was changing, which was required for the sensitivity analysis of their specific contribution to atrial haemodynamics. Finally, tetrahedral volumetric meshes were generated (using Gmsh) from each synthetic surface mesh for the subsequent CFD simulations.

2.3. LAA shape descriptors

We estimated some simple shape descriptors to roughly characterize LAA geometries, inspired on measurements used by clinicians to select the optimal dimensions of the LAAO devices, including: the LAA volume and its number of lobes; the diameters ($DMin$, $DMax$) of the LAA neck/ostium; the height (OsD) and area of the ostium (OsA), equivalent to the landing zone concept (where ideally the LAAO devices should be implanted); a straight line length (H) estimating the depth of the LAA; and $H0$, which is the distance between the middle point of H and the further point of the LAA (i.e. its apex). Figure 3 shows some of these measurements on a patient-specific LAA geometry.

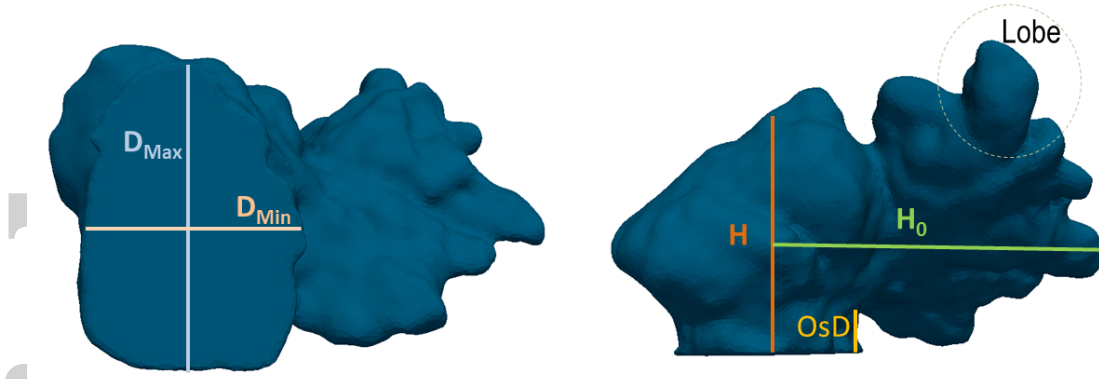


Figure 3. Left atrial appendage (LAA) geometrical parameters: LAA height (H), LAA depth (H_0), maximum and minimum ostium diameters (D_{Max} , D_{Min} , respectively) and depth (OsD).

2.4. Computational Fluid Dynamics model

Computational fluid dynamics (CFD) simulations were run on the 36 different synthetic models. A first order implicit unsteady formulation was used for the solution of the momentum equations in conjunction with a standard partial discretization for the pressure (under-relaxation factors set by default to 0.3 and 0.7 for the pressure and momentum, respectively). Blood flow in the LA was modeled using the incompressible Navier Stokes and continuity equations. Residuals of mass and momentum conservation equations lower than 0.001 were considered as absolute convergence criteria. Blood was modeled as an incompressible Newtonian fluid of density $\rho = 1060 \text{ kg/m}^3$ [15]. The dynamic viscosity of blood in large vessels and the heart at normal physiological conditions is $\mu = 0.0035 \text{ Pa} \cdot \text{s}$ [15]. Simulations were run using a laminar flow hypothesis under isothermal and non-gravitational effects. All walls were simulated rigid and with no-slip conditions, replicating the worst case scenario in AF, without atrial wall contraction. The differential equations were solved using a time-step $\delta t = 0.01 \text{ s}$. At the inlets of the left atrial model (i.e. the four PVs) a time-varying pressure function was applied (see Figure 4) following clinical observations available in Fernandez-Perez et al. [9]. At the outlet (i.e. the mitral valve, MV) a pressure of 8 mmHg [20] was imposed during the ventricular diastolic phase. In ventricular systole, the MV is closed and was simulated as a wall boundary. The systole phase lasted 0.4 s and the diastole phase lasted 0.65 s [9].

Table II. Advanced haemodynamic indices. TAWSS: time-averaged wall shear stress; OSI: Oscillatory shear index; RTT: relative residence time; ECAP: endothelial cell activation potential.

| TAWSS | OSI | ECAP | RTT |
|---------------------------------|---|---------------------|--|
| $\frac{1}{T} \int_0^T WSS dt$ | $\frac{\frac{1}{2} \int_0^T WSS dt}{\int_0^T WSS dt}$ | $\frac{OSI}{TAWSS}$ | $[1 - (2 \cdot OSI) \cdot TAWSS]^{-1}$ |

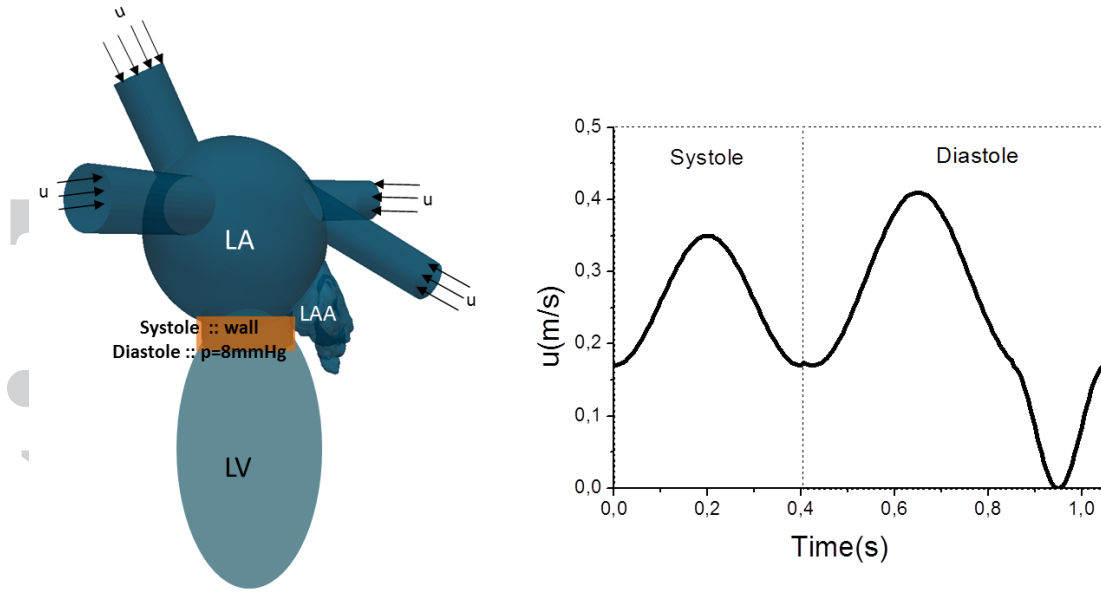


Figure 4. Left: boundary conditions applied to the mitral valve (MV, outlet), consisting in wall conditions during left ventricle (LV) systole and pressure equal to 8 mmHg during diastole. Right: generic blood velocities (u) waveform applied to the pulmonary veins (inlets) during the whole cardiac cycle. LAA: Left Atrial Appendage.

2.5. Haemodynamic descriptors

Velocity streamlines of simulated flows were used to visualize fluid dynamics profiles and vorticity information. Vortex structures were computed calculating the q -criterion [24], obtained using the second invariant of the velocity gradient tensor, aiming at identifying regions with vortices since they could be associated with thrombus formation. Furthermore, we estimated regional statistics (e.g. average and standard deviation) of variables such as flow velocity, strain rate, wall shear stress (WSS), pressure and local Reynolds number for the different LA/LAA configurations in the sensitivity analysis. We also computed several parameters potentially related to the risk of thrombus formation such as the time averaged wall shear stress (TAWSS), the oscillatory shear index (OSI), the relative residence time (RRT) and the endothelial cell activation potential (ECAP), as can be seen in Table II. The TAWSS captures the mechanobiological effects of the WSS in the LAA wall: small values of WSS represent low flow velocities, which are related with blood stasis and higher coagulation risk. The OSI is a nondimensional parameter that has been proved successful in identifying atheroprone regions of human carotid bifurcation [1]. A maximum value of OSI (0.5) corresponds to complex changes of blood flow patterns and can also be related with blood coagulation [?]. The ECAP parameter, defined by Di Achille et al. [1], unifies both TAWSS and OSI variables, being an interesting index highly related with the localization of thrombogenic areas: wall regions exposed to both high OSI and low TAWSS would yield high ECAP values associated with endothelial susceptibility and risk of thrombus formation risk. Finally, the relative residence time

Table III. Shape descriptors for patient-specific left atrial appendage (LAA) geometries. Dmax, Dmin: maximum and minimum ostium diameters, respectively. OsA, OsD: ostium area and depth, respectively. H and H₀: LAA height and depth, respectively.

| Samples | Dmax (mm) | Dmin (mm) | OsA (cm^2) | OsD (mm) | H ₀ (mm) | H (mm) | Lobes Lobes | Volume (mL) |
|----------|--------------|--------------|-------------------|-------------|------------------------|-----------|----------------|----------------|
| Sample 1 | 31.5 | 24.6 | 6.08 | 3.0 | 39.9 | 21.2 | 3 | 16.95 |
| Sample 2 | 24.5 | 16.2 | 3.12 | 4.8 | 31.6 | 18.0 | 7 | 8.66 |
| Sample 3 | 32.9 | 23.8 | 6.15 | 8.0 | 35.8 | 19.5 | 0 | 14.77 |
| Sample 4 | 32.9 | 22.4 | 5.79 | 3.0 | 32.3 | 19.8 | 5 | 13.42 |

(RRT) parameter proposed by Himburg et al. [12], combines WSS and OSI to reflect the residence time of blood particles near the wall.

2.6. Sensitivity and statistical analysis

The sensitivity and statistical analysis was run on the 36 synthetic LA/LAA configurations that combined the different morphological descriptors under study. Three different levels (average, avg; maximum, max; minimum, min) were used for the LA volume and PVs-MV areas, as can be seen in Table I). To reduce the number of results and combinations, we choose to simultaneously apply the same level to PV and MV areas for each experiment. Therefore, the number of experiments after the combination of these three variables was equal to $3^2 = 9$ (see Table I). In addition, the type of LAA morphology (i.e. the four different samples) was a qualitative variable that increased the number of experiments to 36, nine different LA configurations for each LAA. The statistical analysis was carried out using a multivariable ANOVA, estimating the main effect of LA/LAA shape descriptors on the haemodynamics ones based on the statistically significant value ($p < 0.05$), after Bonferroni estimation. Values used for the statistical analysis corresponded to the 90th percentile of each haemodynamics variable, integrated over the LAA surfaces. These values meant that 10% of LAA surface attained higher magnitudes than the 90th percentile one. Left atrial appendage ostium velocities were consistently obtained for all points belonging to the same plane for all samples (around 1 to 3 mm away from the interface between the LA and LAA); only the maximum velocity value at end-diastole was kept for the subsequent statistical analysis.

3. RESULTS

In this section, shape and haemodynamic descriptors obtained in all experiments of the sensitivity analysis will be described, focusing on the influence of LAA morphology and LA environment in blood flow patterns.

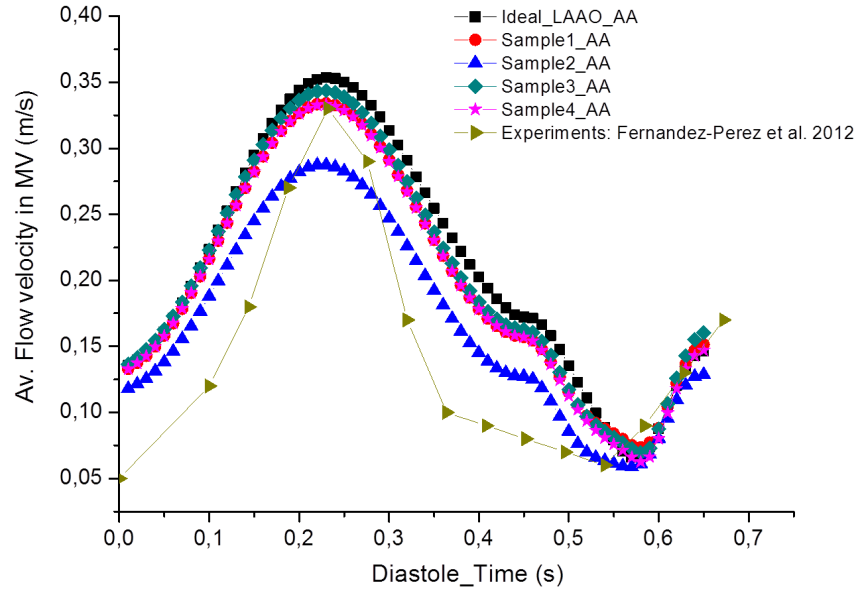


Figure 5. Mitral valve spatial average outflow velocity for different left atrial appendage (LAA) morphologies (Sample 1-4) with the average dimensions (AA) of all remaining morphological parameters (pulmonary veins and mitral valve areas, LA volume), including one case without LAA (LAAO) simulating its occlusion. As a reference, the mitral valve inflow velocity pattern from Fernandez-Perez et al. [9] is also plotted.

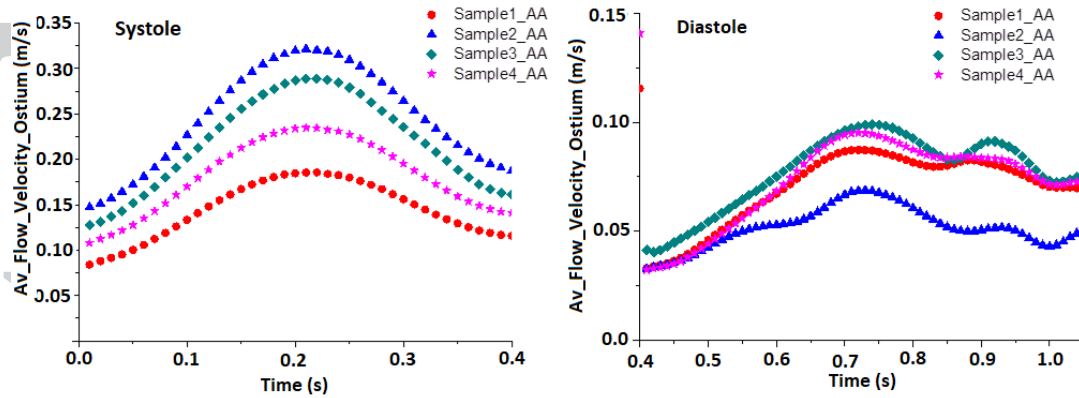


Figure 6. Average blood flow velocity in the ostium of the four different LAA morphologies (remaining shape descriptors fixed to average values, AA). a) Systole; b) Diastole.

3.1. Shape descriptors

Table III gathers the shape descriptors estimated for the four chosen patient-specific LAA geometries. Sample 2 had the lowest volume and the smallest dimensions in several parameters (ostium dimensions, LAA distances), while having the largest number of lobes. Sample 1 had the largest LAA volume and from the ostium to the apex lengths. Sample 3 was the smoothest (zero lobes) and the one with the largest ostium depth (OsD). Three experts independently classified the studied LAA morphologies into each one of the four classical categories (chicken wing, windsock, cactus and cauliflower; see descriptions in Appendix 1). However, complete consensus was reached just in one of them, Sample 4 in the cactus category. For the remaining LAA morphologies, we

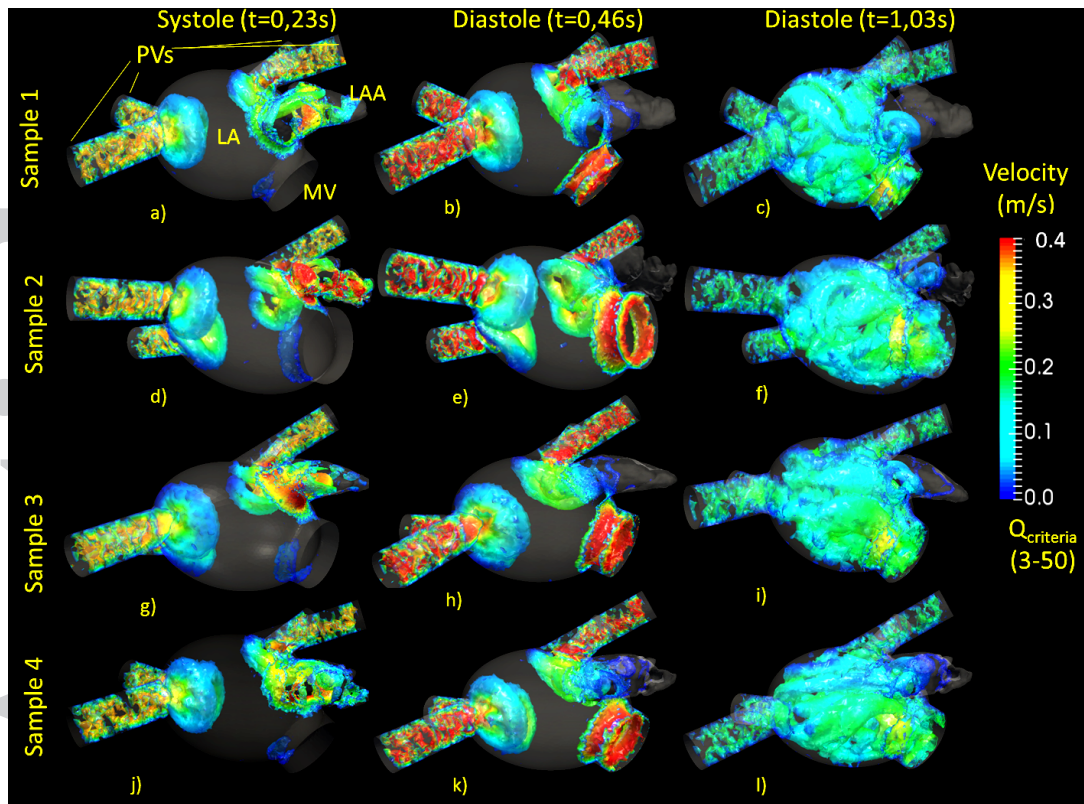


Figure 7. Vortex structures during systole and diastole in the timepoints reaching maximum velocity peaks. Four samples in the times 0.23 s, 0.46 s and 1.03 s. The visualization of vortex were created computing the q -criteria and applying the range $3-50 \text{ s}^{-2}$. The color map corresponds to the velocity magnitude.

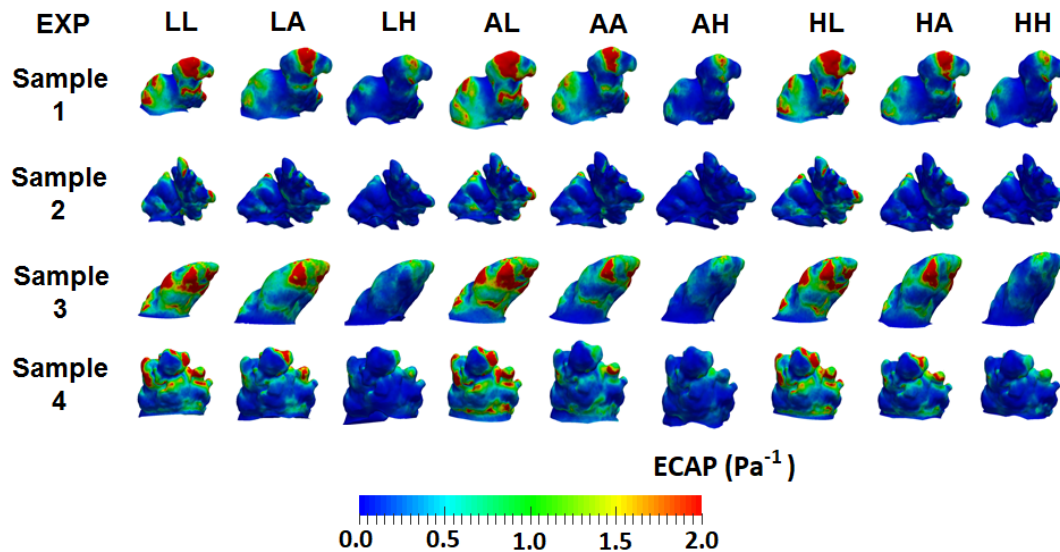


Figure 8. Endothelial cell activation potential (ECAP) index distribution map for different left atrial appendage (LAA) morphologies (Sample 1-4) and pulmonary veins / mitral valve (PV-MV) experiments (EXP). The first and second index of experiment notation indicate the magnitude of LA volume and PV-MV dimensions, respectively. Levels and magnitude: low (L), average (A) and high (H).

obtained: Sample 1, 2/3 experts labelled it as windsock and one as cactus; Sample 2, 2/3 experts labelled it as cauliflower and one as cactus; and Sample 3, each expert labelled it differently as cauliflower, chicken wing and windsock.

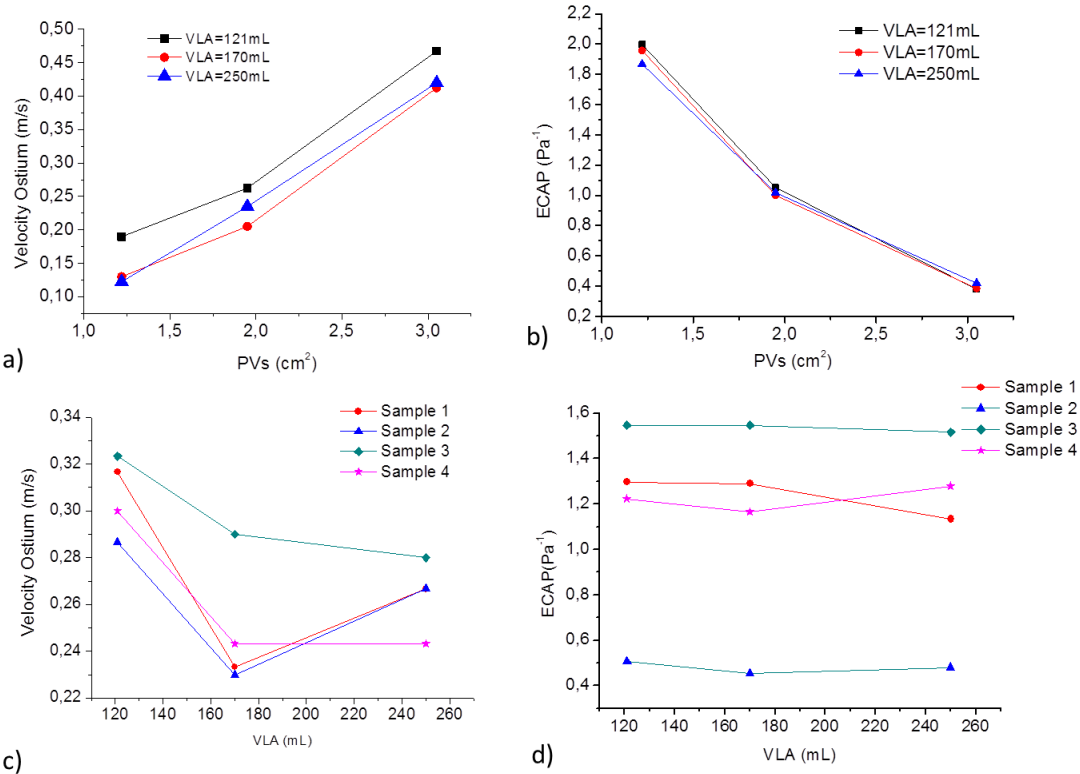


Figure 9. Averaged values over all experiments of left atrial appendage (LAA) ostium blood flow velocities (a,c) and endothelial cell activation potential (ECAP, b,d). Top row: influence of pulmonary vein size on the three different LA volume (LAV) configurations. Bottom row: influence of LA volume for the four different LAA morphologies.

3.2. Haemodynamics descriptors

3.2.1. Influence of LAA morphology on haemodynamics In the first experiments of the sensitivity analysis the only varying morphological parameter was the LAA, fixing the remaining LA structures (i.e. LA volume and PV-MV configuration). The mitral valve blood outflow profiles during diastole in four experiments with the same LA configuration (average values, AA) and different LAA morphologies, including one case without LAA (LAAO) to simulate its occlusion, are plotted in Figure 5. As a reference, the mitral valve inflow velocity pattern obtained by Fernandez-Perez et al. [9], from where PV boundary conditions were taken, is also shown. These patterns represent the filling process of the left ventricle and can be related with gradient pressure and dysfunction of the mitral valve. Figure 5 exposes the three phases of diastole in the LA: the E wave, a short low blood flow period and the final atrial contraction. Sample 2 LAA morphology generated slightly lower mitral valve flow peak velocities than the remaining ones, including the LAAO case. The E/A wave values from these curves were: 2.20 for Sample 1; 2.23 for Sample 2; 2.14 for Sample 3 (the lowest); 2.26 for Sample 4; and 2.41 for synthetic LAAO (the highest). As a reference, the E/A wave value obtained by Fernandez Perez from clinical experiments was 1.94, as seen in Figure 5.

Table IV. Summary of haemodynamics descriptors for all sensitivity analysis configurations. Left atrial appendage ostium velocity values under 0.20 m/s are emphasized since they are related to a higher risk of thrombus formation. Levels and magnitude: low (L), average (A) and high (H). LAV: LA volume. PV: pulmonary veins. MV: mitral valve. TAWSS: time-averaged wall shear stress; OSI: Oscillatory shear index; RTT: relative residence time; ECAP: endothelial cell activation potential.

| Samples | Experiment | | | Maximum velocity in Ostium (m/s) | TAWSS (Pa) | OSI (-) | RRT (s) | ECAP (Pa ⁻¹) |
|----------|------------|----|----|-------------------------------------|---------------|------------|------------|-----------------------------|
| | LAV | PV | MV | | | | | |
| Sample 1 | L | L | | 0.19 | 0.58 | 0.28 | 28.33 | 2.40 |
| | L | A | | 0.26 | 1.05 | 0.28 | 13.08 | 1.09 |
| | L | H | | 0.50 | 2.24 | 0.25 | 4.88 | 0.40 |
| | A | L | | 0.11 | 0.49 | 0.26 | 26.89 | 2.22 |
| | A | A | | 0.20 | 0.73 | 0.29 | 13.3 | 1.22 |
| | A | H | | 0.39 | 1.73 | 0.26 | 4.76 | 0.43 |
| | H | L | | 0.12 | 0.61 | 0.25 | 24.22 | 2.02 |
| | H | A | | 0.23 | 1.14 | 0.26 | 11.38 | 0.91 |
| | H | H | | 0.45 | 2.06 | 0.27 | 5.09 | 0.47 |
| Sample 2 | L | L | | 0.20 | 1.47 | 0.21 | 8.39 | 0.87 |
| | L | A | | 0.23 | 2.40 | 0.24 | 3.69 | 0.40 |
| | L | H | | 0.43 | 4.83 | 0.28 | 2.25 | 0.25 |
| | A | L | | 0.10 | 1.27 | 0.20 | 8.23 | 0.77 |
| | A | A | | 0.16 | 1.89 | 0.21 | 3.78 | 0.39 |
| | A | H | | 0.43 | 4.72 | 0.24 | 1.84 | 0.20 |
| | H | L | | 0.12 | 1.34 | 0.20 | 8.29 | 0.79 |
| | H | A | | 0.22 | 2.48 | 0.22 | 3.67 | 0.39 |
| | H | H | | 0.40 | 4.33 | 0.25 | 2.18 | 0.25 |
| Sample 3 | L | L | | 0.17 | 0.50 | 0.32 | 32.59 | 2.53 |
| | L | A | | 0.29 | 1.08 | 0.33 | 16.67 | 1.65 |
| | L | H | | 0.51 | 2.78 | 0.31 | 4.23 | 0.46 |
| | A | L | | 0.18 | 0.68 | 0.30 | 31.98 | 2.72 |
| | A | A | | 0.26 | 1.22 | 0.32 | 15.76 | 1.46 |
| | A | H | | 0.43 | 2.36 | 0.30 | 4.62 | 0.46 |
| | H | L | | 0.12 | 0.57 | 0.28 | 29.75 | 2.53 |
| | H | A | | 0.27 | 1.36 | 0.30 | 17.34 | 1.59 |
| | H | H | | 0.45 | 2.77 | 0.27 | 4.63 | 0.43 |
| Sample 4 | L | L | | 0.20 | 0.71 | 0.30 | 26.18 | 2.19 |
| | L | A | | 0.27 | 1.50 | 0.31 | 10.57 | 1.07 |
| | L | H | | 0.43 | 2.75 | 0.30 | 3.90 | 0.41 |
| | A | L | | 0.13 | 0.63 | 0.30 | 24.64 | 2.12 |
| | A | A | | 0.20 | 0.88 | 0.28 | 9.89 | 0.93 |
| | A | H | | 0.40 | 2.31 | 0.31 | 4.19 | 0.45 |
| | H | L | | 0.13 | 0.65 | 0.28 | 24.51 | 2.13 |
| | H | A | | 0.22 | 1.20 | 0.28 | 12.12 | 1.18 |
| | H | H | | 0.38 | 2.26 | 0.30 | 4.95 | 0.53 |

Figure 6 shows blood flow velocity traces in the LAA ostium for the experiments described above (only varying LAA morphology), both in systole and diastole. The observed flow patterns followed the same behaviour than the imposed inlet boundary condition in the pulmonary veins but there were differences between the four LAA morphologies. In systole, Sample 2 and Sample 1 presented the highest (0.32 m/s) and lowest (0.18 m/s) velocity peak values. Interestingly, Sample 2 and Sample 1 had the smallest and largest LAA ostium area, respectively. Nevertheless, flow velocities and morphological descriptors do not hold a unique and linear relation, especially over time. Mitral valve opening in diastole drives blood flow towards the LV through the MV, thus reducing blood volume

penetrating the LAA and considerably changing flow behavior from systole, as it can be appreciated in Figure 6. During diastole, Sample 2 was the LAA geometry that reached the lowest ostium velocities (0.07 m/s). Nevertheless, the four LAA morphologies had LAA ostium peak velocities in diastole below the threshold ($< 0.2 \text{ m/s}$) that is associated with a high risk of thrombus formation.

Given that during systole the MV is closed, blood flow did not exit the LA during this phase and a great amount of blood entered the LAA, substantially more than during diastole, as can be seen in Figure 7. This figure depicts vorticity maps for the experiments only varying LAA morphologies (Sample 1-4) in timepoints within the cardiac cycle reaching maximum velocity peaks. The presence of vortices within the LAA constitute an important haemodynamics characteristic since they are found in regions with complex flows, thus with an increased risk of thrombus formation, in particular when combined with low velocities (see videos in Appendix 2). Figure 7 also shows that during LA filling (systole) the highest velocities appear inside the LAA. Later, during the passive LV filling (diastole, 0.46s) highest velocities are found in the MV. Finally, in LA contraction (last part of diastole) the number of vortices increased, appearing all over the atrial chamber. Sample 4 is the LAA morphology with more vortices associated to low velocities during systole, suggesting a higher risk for thrombus formation, comparing to the other LAA.

The reduced LAA blood flow, especially in diastole, induced low velocity and WSS magnitudes that yielded low TAWSS and greater WSS vector deflection, increasing the OSI. Both events led to increased ECAP and RRT values, thus increasing the risk of thrombus formation, in particular in the most distant LAA regions (i.e. close to the apex), as can be seen in Figure 8. Moreover, LAA morphologies with lobes attained extremely high ECAP values in these regions as they induced complex flow patterns and were reached by scant blood flow.

3.2.2. Influence of LA environment on haemodynamics LAA 90th percentile values of the haemodynamic descriptors (TAWSS, OSI, RTT, ECAP; see complete cumulative plot in Appendix 3 Figure 10; 11; 12; 13), together with peak velocities in LAA ostium are shown in Table IV. Experiments with small PVs and MV areas (L in Table IV) were consistently associated with the lowest LAA velocities, being below 0.2 m/s, thus with a high risk of thrombus formation [3]. These low velocity values in LAA ostium corresponded to high values of ECAP and RRT inside the appendage. Values of RRT and ECAP were also influenced by the morphology and volume of the LAA. For instance, Sample 2 attained the lowest values of RRT and ECAP, arguably due to its smallest size and the small mechanical stimuli. This is in agreement to observations from Figure 8, where Sample 1, 3 and 4 present larger regions with higher ECAP values (red in the figure) than Sample 2. It can also be appreciated that the ECAP distribution did not seem linearly related to the amount of secondary lobes (e.g. Sample 2 is the one having more lobes).

Finally, Figure 9 shows the averaged values over all experiments of LAA ostium blood flow velocities and ECAP values when only changing PV size for the three different LA volumes and when only changing LA volume for the four different LAA morphologies. From the figure, we can observe that PV size has a larger influence on LAA ostium velocities and ECAP values than LA volume, confirming the importance of LA configuration to direct blood flow towards the LAA. Figure 9 also shows a critical role of LAA morphology, especially in ECAP values.

4. DISCUSSION AND CONCLUSIONS

LAA thrombi pathogenesis has not been fully elucidated yet, due to the biological, physical and anatomical complexity in this atrial structure. Despite the high percentage of thrombi formation in the LAA of AF patients, the current existing data, mainly from medical images, relating LAA morphology and blood flow with thrombi formation are too simplistic for evaluating the risk of thromboembolic events in these patients. For elucidating this phenomenon, we have developed a pipeline with 3D CFD simulations that estimates advanced haemodynamical characterization indices that can be related to morphological descriptors. Furthermore, the developed sensitivity analysis framework, generating tens of synthetic LA/LAA configurations, enabled the individualized study of the influence of each one of these morphological descriptors, something unachievable with the analysis of complex clinical data. The present study evaluates the influence of LA and LAA anatomical variations in blood flow patterns and their relation with thrombi formation. An automatization of these measurements could lead to an improvement of LAAO devices selection and to a prior determination of thrombus generation risk. Four different LAA morphologies were studied, where experts could not reach a consensus on their assignment into the classical classification [5]. The difficulties for obtaining full agreement among experts/clinicians on this LAA morphological classification suggest to be cautious when relating some morphologies (i.e. chicken wing) with a reduced risk of thrombus formation. From a mechanical point of view, it makes sense that a smoother and more regular LAA morphology should be associated with less complex blood flows and with higher velocities. However, it is also as important to consider the LA configuration around the LAA for a better morphological characterization. Our results point at the need of using a combination of advanced morphological descriptors, including LA and LAA ones, rather than a classification for determining the LAA coagulation risk [26].

Isolating the LAA influence from the rest of the LA variables it was observed that the LAA ostium area (OsA) played a major role in regulating velocities within the appendage due to the continuity and momentum conservation equations during systole. Lower OsA values yielded high

velocities within the LAA, usually associated with a low risk of thrombus formation. Such was the case of Sample 2, which exhibited the highest LAA velocities. Differently, Sample 3 had the highest OsA and consequently the lowest velocities, this time associated with a higher risk of thrombi formation. Lee et al. [17] recently proposed that ostium diameter and blood flow velocity were the main parameters influencing thrombus formation. They suggested ostium areas higher than 3.5 cm^2 and velocities less than 37 cm/s were under higher risk. They also proposed LAA orifice areas higher than 4 cm^2 and velocities lower than 40 cm/s as independent stroke predictors. In terms of LAA orifice area, we reached the same conclusion, given that Sample 2 ($\text{OsA} = 3.12 \text{ cm}^2$) exhibited less thrombogenic risk. However, the combinations of different factors is more relevant than the effect of an individual parameter.

In addition, LAA volume also played an important role in regulating coagulation risk. Appendages with lower LAA volume (e.g. Sample 2 and Sample 3) were less prone to exhibit high ECAP values compared with those of higher volume, since high blood flow volume with high enough velocities can reach all LAA regions in an homogeneous way. These results are in agreement with findings by Yaghi et al. [31]; they showed that large left atrial volumes were associated with stroke risk, arising stasis conditions attributed to rouleaux formation. Furthermore, some studies claimed that multi-lobar atrial appendage morphology may favor blood stasis. Al-Saady et al. [2] suggested the long, blind ended trabeculae pouch as potential candidates for blood stagnation. The number of lobes has also been shown to be an independent risk factor for thrombus presence [32]. However, among the LAAs in our study the one with seven lobes (Sample 2) attained the lowest blood coagulation risk due to other factors (e.g. OsA and LAA volume), which have a direct influence on blood flow within the appendage.

One of the most relevant findings from our sensitivity analysis is the critical role of the pulmonary vein configuration, being the morphological parameter with more influence on LAA haemodynamics. An increment in PV size, independently of the LAA morphology, is translated into an increase in the incoming LA blood volume and, thus, flow velocity in the ostium, reducing the risk of thrombus formation. LAA morphology influence was amplified with PV size. Velocity magnitudes were directly related to blood volume-to-LA volume aspect ratio. When the LA volume increased, ostium velocities decreased when PV dimensions were maintained. These results could represent a change of paradigm in how risk of thrombus formation is studied with respect to the LAA morphology and blood flow velocities; LA configuration including PV patterns should be taken into account when analysing clinical data from AF patients for the assessment of the risk of thrombus formation.

Future work will be focused on a more detailed study of different PV patterns and its relation with blood haemodynamics, as well as increasing the number of studied LAA to get enough statistical

power to draw more robust conclusions on the impact of LAA morphology in atrial blood flow and the risk of thrombus formation.

Accepted Article

5. ACKNOWLEDGEMENTS

This work was partly supported by COMPILAAO Retos I+D project (DPI2015-71640-R) and the Fundacio La Marato de TV3 (20154031).

Accepted Article

6. BIBLIOGRAPHY

A. APPENDIX SECTION

A.1. Appendix 1: full description of morphological and haemodynamic indices for the four studied LAA morphologies.

A.1.1. Sample 1 Sample 1 was the appendage with the highest volume, a relatively high OsA and three lobes (Table 3). It presented an average MV output velocity profile (Figure 5). Its ostium velocities during systole were the lowest and average low during diastole (Figure 6). Several vortex structures were found within the appendage during systole with relatively high velocities and some of them during diastole with low velocities distal to the ostium region (Figure 7). High ECAP value regions were found next to apex regardless of the LA configuration (Figure 8). In LA conformations with less thrombogenic tendency, ECAP distribution was maintained but with reduced magnitudes.

A.1.2. Sample 2 Sample 2 was the smallest appendage with seven lobes and a volume magnitude half the value of Sample 1 (Table 3). Its MV outlet velocities (Figure 5), overall dimensions and ostium area were the lowest. Consequently, ostium systolic velocities were the highest, whilst diastolic the lowest (Figure 6). During systole, a high number of vortex structures were identified all over the LAA with highest velocities than the other samples (Figure 7). In addition, it always exhibited the lowest ECAP values compared with the rest of samples independently of its LA configuration (Figure 8).

A.1.3. Sample 3 Sample 3 appendage had high volume, no lobes and the greatest OsA (Table 3). MV outlet velocities were similar to those of sample 1, 4 and LAAO (Figure 5). Ostium systolic velocities were average whilst diastolic were the highest but not far from samples 1 and 4 (Figure 6). Vorticities with high velocity values were identified during systole near the ostium and some near the apex with lower velocities. During diastole, some vortex structures with low velocities originated in the LAA, near the ostium region (Figure 7).

A.1.4. Sample 4 Sample 4 attained the highest ECAP values due to its high volume and OsA, specially near the apex (Figure 8). This appendage also had the highest 90th percentile value, meaning that high ECAP values had higher prevalence than in the rest of samples (Table 4). Sample 4 had five lobes and average volume and dimensions (Table 3). MV and ostium velocities were average for both systole and diastole (Figure 5 and Figure 6). It was the appendage morphology exhibiting the highest amount of low velocity vorticities during diastole (Figure 7). It attained high ECAP values but with lower prevalence than sample 1 and 3 (Figure 8).

A.2. *Appendix 2: videos of vorticity maps in systolic and diastolic phases for each LAA morphology.*

Videos of dynamic vorticity maps in systolic and diastolic phases with average LA configuration and for each LAA morphology, showing the time dependence of blood flow in the models.

A.3. *Appendix 3: Cumulative Histogram for main haemodynamic descriptors for each LAA morphology.*

REFERENCES

1. P Di Achille, G Tellides, C A Figueroa, J D Humphrey, Proc R Soc A, P Di Achille, G Tellides, and C A Figueroa. A haemodynamic predictor of intraluminal thrombus formation in abdominal aortic aneurysms A haemodynamic predictor of intraluminal thrombus formation in abdominal aortic aneurysms. (October), 2014.
2. N. M. Al-Saady, O. A. Obel, and A. J. Camm. Left atrial appendage: structure, function, and role in thromboembolism. *Heart*, 82:547–555, 1999.
3. Roy Beigel, Nina C. Wunderlich, Siew Yen Ho, Reza Arsanjani, and Robert J. Siegel. The left atrial appendage: Anatomy, function, and noninvasive evaluation. *JACC: Cardiovascular Imaging*, 7(12):1251–1265, 2014.
4. David S Beutler, Richard D Gerkin, and Akil I Loli. The Morphology of Left Atrial Appendage Lobes: A Novel Characteristic Naming Scheme Derived through Three-Dimensional Cardiac Computed Tomography. *World Journal of Cardiovascular Surgery*, 04(03):17–24, 2014.
5. Luigi Di Biase, Pasquale Santangeli, Matteo Anselmino, Prasant Mohanty, Ilaria Salvetti, Sebastiano Gili, Rodney Horton, Javier E. Sanchez, Rong Bai, Sanghamitra Mohanty, Agnes Pump, Mauricio Cereceda Brantes, G. Joseph Gallingerhouse, J. David Burkhardt, Federico Cesarani, Marco Scaglione, Andrea Natale, and Fiorenzo Gaita. Does the Left Atrial Appendage Morphology Correlate With the Risk of Stroke in Patients With Atrial Fibrillation? *Journal of the American College of Cardiology*, 60(6):531–538, aug 2012.
6. Petter Dyverfeldt, Malenka Bissell, Alex J Barker, Ann F Bolger, Carl-Johan Carlhäll, Tino Ebbers, Christopher J Francios, Alex Frydrychowicz, Julia Geiger, Daniel Giese, Michael D Hope, Philip J Kilner, Sebastian Kozerke, Saul Myerson, Stefan Neubauer, Oliver Wieben, and Michael Markl. 4D flow cardiovascular magnetic resonance consensus statement. *Journal of cardiovascular magnetic resonance : official journal of the Society for Cardiovascular Magnetic Resonance*, 17(1):72, 2015.
7. Günther Ernst, Claudia Stöllberger, Friedrich Abzieher, Walter Veit-Dirscherl, Elisabeth Bonner, Brigitte Bibus, Barbara Schneider, and Jörg Slany. Morphology of the left atrial appendage. *The Anatomical Record*, 242(4):553–561, aug 1995.
8. Diane Fatkin, Raymond P. Kelly, and Michael P. Feneley. Relations between left atrial appendage blood flow velocity, spontaneous echocardiographic contrast and thromboembolic risk in vivo. *Journal of the American College of Cardiology*, 23(4):961–969, 1994.
9. G. C. Fernandez-Perez, R. Duarte, M. Corral de la Calle, J. Calatayud, and J. Sanchez Gonzalez. Analysis of left ventricular diastolic function using magnetic resonance imaging. *Radiologia*, 54(4):295–305, 2012.
10. Xavier Freixa, Jason L.K. Chan, Apostolos Tzikas, Patrick Garceau, Arsene Basmadjian, and Reda Ibrahim. The Amplatzer Cardiac Plug 2 for left atrial appendage occlusion: novel features and first-in-man experience. *EuroIntervention*, 8(9):1094–1098, jan 2013.

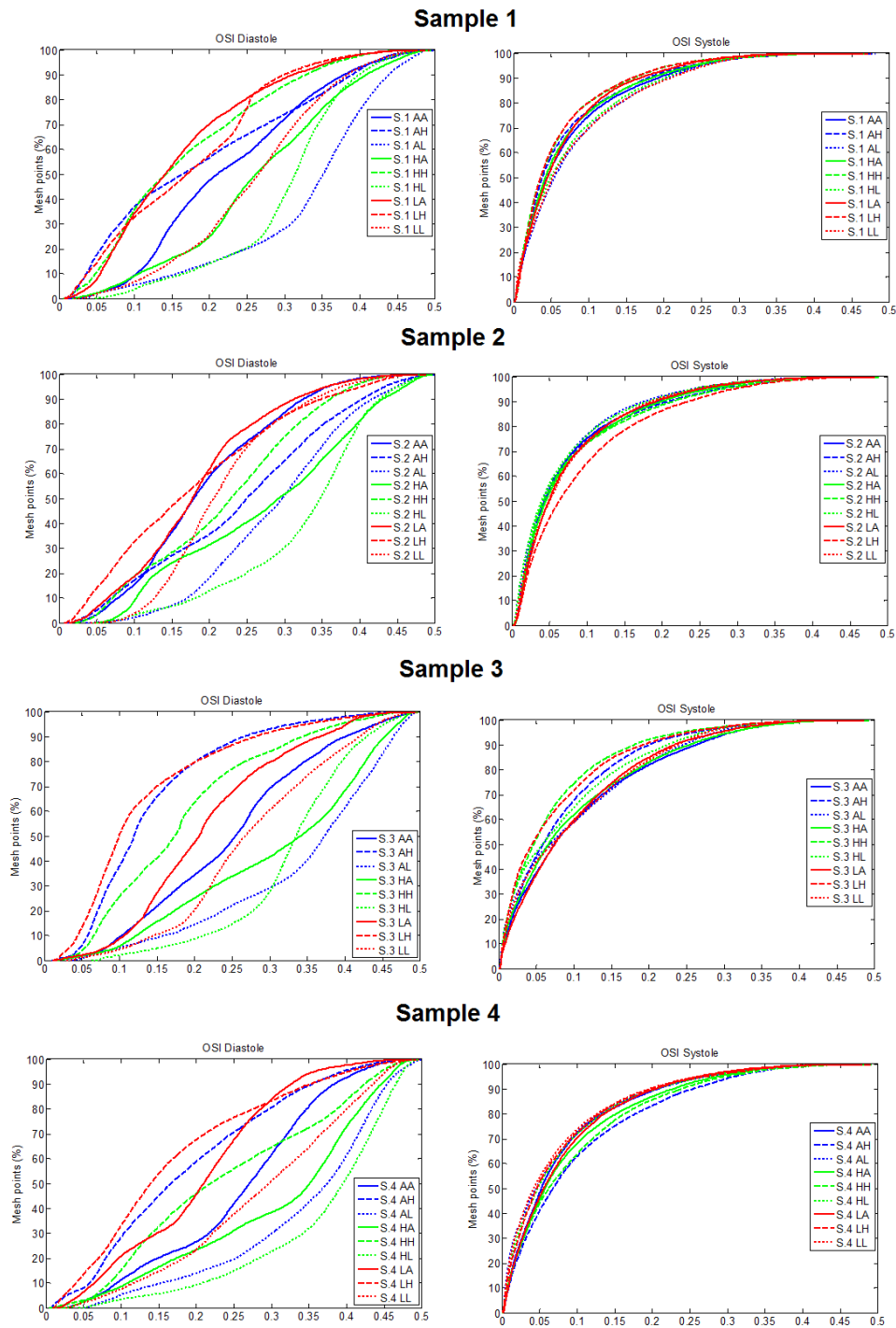


Figure 10. Cumulative Histogram for oscillatory shear index (OSI) for the four LAA morphologies (Sample 1-4). Left and right column show diastole and systole cardiac phases, respectively.

11. Keiko Fukushima, Noritoshi Fukushima, Ken Kato, Koichiro Ejima, Hiroki Sato, Kenji Fukushima, Chihiro Saito, Keiko Hayashi, Kotaro Arai, Tetsuyuki Manaka, Kyomi Ashihara, Morio Shoda, and Nobuhisa Hagiwara. Correlation between left atrial appendage morphology and flow velocity in patients with paroxysmal atrial fibrillation. *European Heart Journal Cardiovascular Imaging*, page jev117, may 2015.
12. H A Himburg, D M Grzybowski, A L Hazel, J A LaMack, X M Li, and M H Friedman. Spatial comparison between wall shear stress measures and porcine arterial endothelial permeability. *Am J Physiol Heart Circ Physiol*,

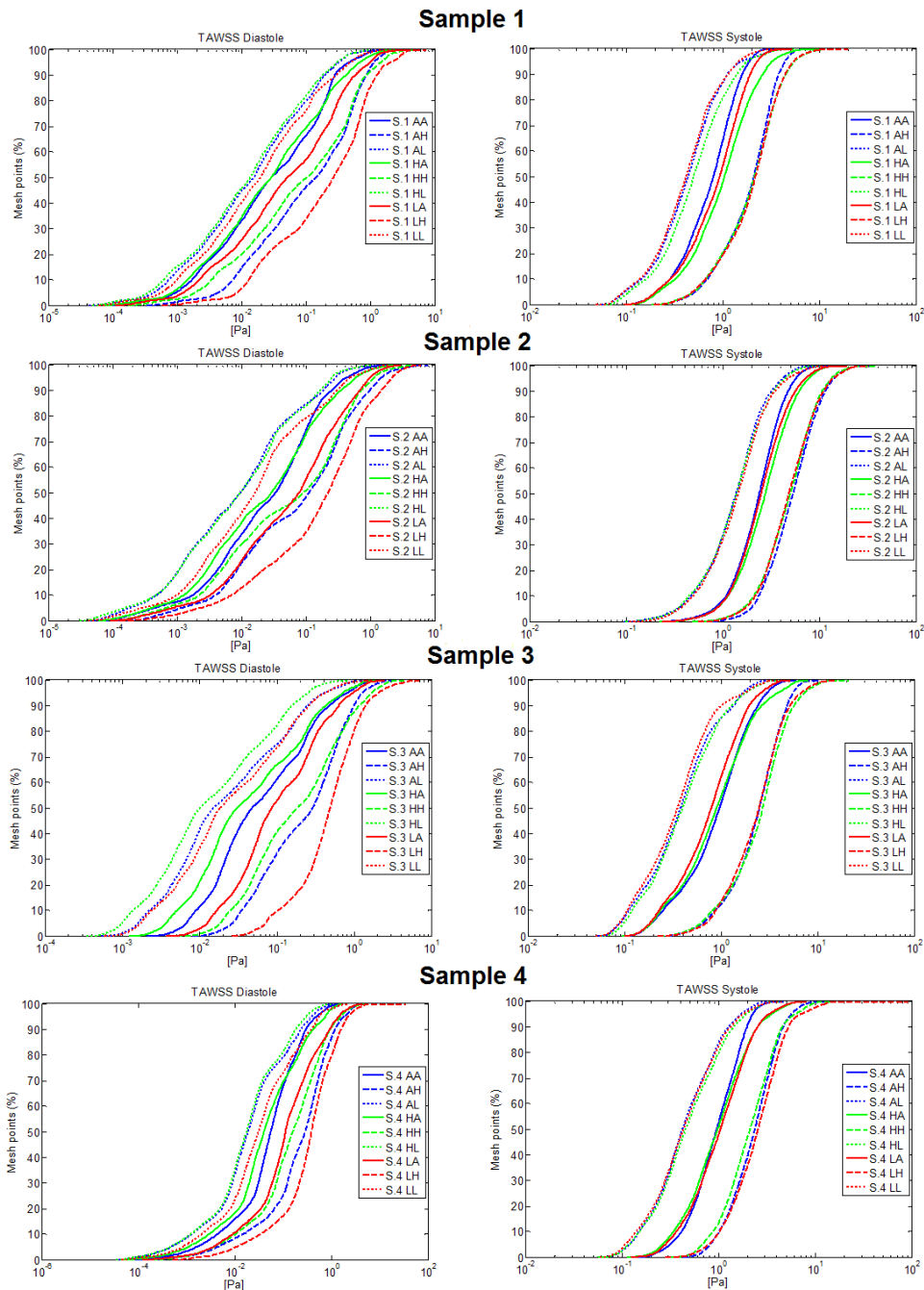


Figure 11. Cumulative Histogram for time-averaged wall shear stress (TAWSS) for the four LAA morphologies (Sample 1-4). Left and right column show diastole and systole cardiac phases, respectively.

286(5):H1916–22, 2004.

13. Irfan M. Khurram, Jane Dewire, Michael Mager, Farhan Maqbool, Stefan L. Zimmerman, Vadim Zipunnikov, Roy Beinart, Joseph E. Marine, David D. Spragg, Ronald D. Berger, Hiroshi Ashikaga, Saman Nazarian, and Hugh Calkins. Relationship between left atrial appendage morphology and stroke in patients with atrial fibrillation. *Heart Rhythm*, 10(12):1843–1849, dec 2013.
14. Ryo Koizumi, Kenichi Funamoto, Toshiyuki Hayase, Yusuke Kanke, Muneichi Shibata, Yasuyuki Shiraishi, and Tomoyuki Yambe. Numerical analysis of hemodynamic changes in the left atrium due to atrial fibrillation. *Journal of Biomechanics*, 48(3):472–478, feb 2015.

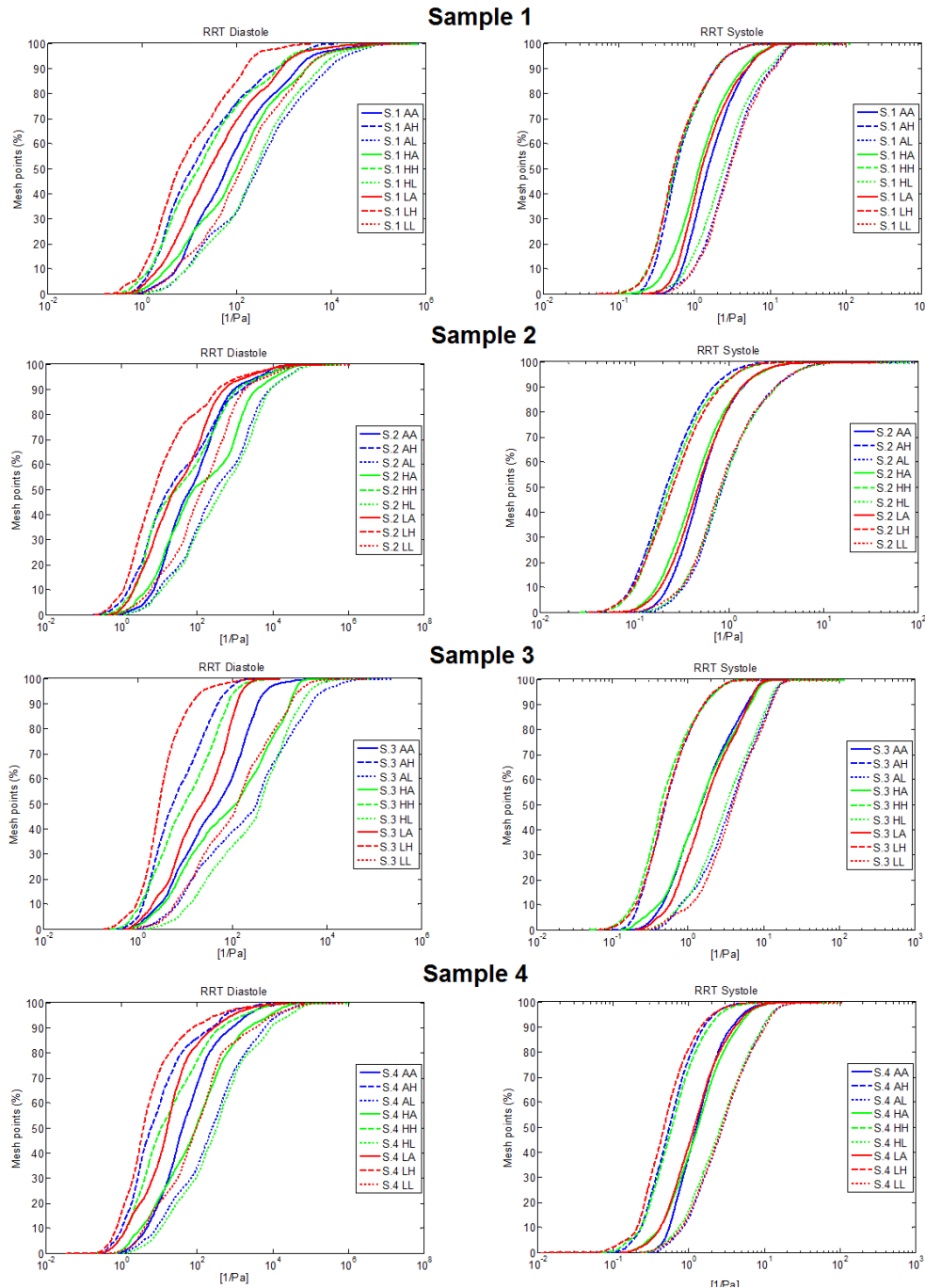


Figure 12. Cumulative Histogram for relative residence time (RRT) for the four LAA morphologies (Sample 1-4). Left and right column show diastole and systole cardiac phases, respectively.

15. D. N. Ku, D. P. Giddens, C. K. Zarins, and S. Glagov. Pulsatile flow and atherosclerosis in the human carotid bifurcation. Positive correlation between plaque location and low oscillating shear stress. *Arteriosclerosis, Thrombosis, and Vascular Biology*, 5(3):293–302, 1985.
16. Y Y Lam. A new left atrial appendage occluder (Lifetech LAmbré Device) for stroke prevention in atrial fibrillation. *Cardiovasc Revasc Med*, 14(3):134–136, 2013.
17. Jung Myung Lee, Jin-Bae Kim, Jae-Sun Uhm, Hui-Nam Pak, Moon-Hyoung Lee, and Boyoung Joung. Additional value of left atrial appendage geometry and hemodynamics when considering anticoagulation strategy in patients

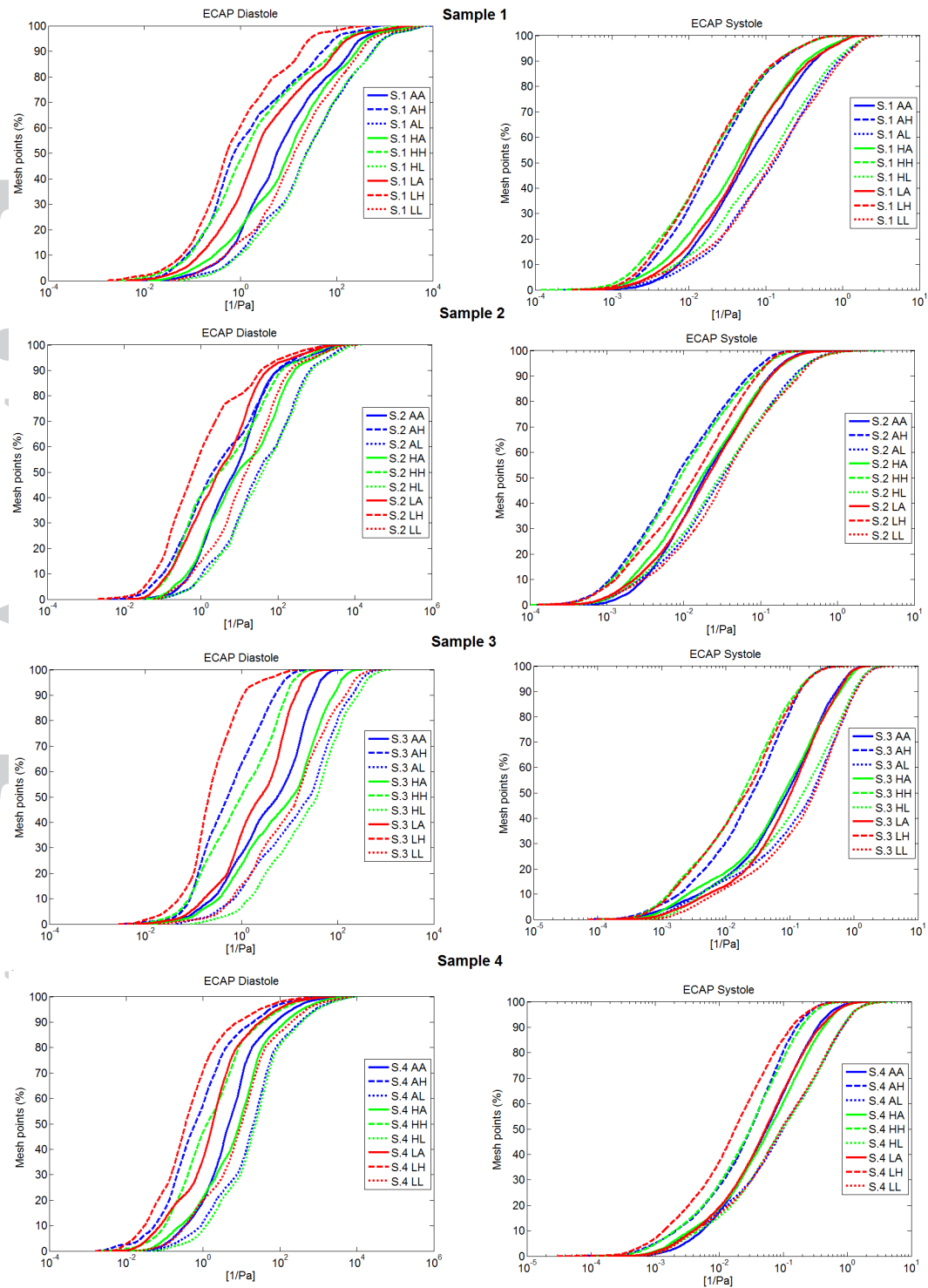


Figure 13. Cumulative Histogram for endothelial cell activation potential (ECAP) for the four LAA morphologies (Sample 1-4). Left and right column show diastole and systole cardiac phases, respectively.

with atrial fibrillation with low CHA₂DS₂-VASc scores. *Heart Rhythm*, 14(9):1297–1301, 2017.

18. Jung Myung Lee, Jiwon Seo, Jae-Sun Uhm, Young Jin Kim, Hye-Jeong Lee, Jong-Youn Kim, Jung-Hoon Sung, Hui-Nam Pak, Moon-Hyoung Lee, and Boyoung Joung. Why Is Left Atrial Appendage Morphology Related to Strokes? An Analysis of the Flow Velocity and Orifice Size of the Left Atrial Appendage. *Journal of Cardiovascular Electrophysiology*, 26(9):922–927, sep 2015.

19. Michael Markl, Daniel C Lee, Nicholas Furiasse, Maria Carr, Charles Foucar, Jason Ng, James Carr, and Jeffrey J Goldberger. Atrial Structure and Function Left Atrial and Left Atrial Appendage 4D Blood Flow Dynamics in Atrial Fibrillation. pages 1–10, 2016.
20. Sherif F Nagueh, Christopher P Appleton, Thierry C Gillebert, Paolo N Marino, Jae K Oh, Otto A Smiseth, Alan D Waggoner, Frank A Flachskampf, Patricia A Pellikka, and Arturo Evangelisa. Recommendations for the Evaluation of Left Ventricular Diastolic Function by Echocardiography. *European Journal of Echocardiography*, 10(2):165–193, aug 2008.
21. Sotirios Nedios, Jelena Kornej, Emmanuel Koutalas, Livio Bertagnolli, Jędrzej Kosiuk, Sascha Rolf, Arash Arya, Philipp Sommer, Daniela Husser, Gerhard Hindricks, and Andreas Bollmann. Left atrial appendage morphology and thromboembolic risk after catheter ablation for atrial fibrillation. *Heart Rhythm*, 11(12):2239–2246, 2014.
22. Andy L Olivares, Guadalupe Garcia-Isla, Etelvino Silva, Marta Nuñez-Garcia, Constantine Butakoff, Damián Sánchez-quintana, Xavier Freixa, Jérôme Noailly, and Camara Oscar De Potter, Tom. Combined analysis of virtual haemodynamics patterns and LAA morphologies in relation with the risk of thrombus formation. *European heart journal*, 38(Issue suppl_1):ehx501.86, 2017.
23. Andy L Olivares, Etelvino Silva, Marta Nuñez-Garcia, Constantine Butakoff, Damián Sánchez-quintana, Xavier Freixa, Jérôme Noailly, and Camara Oscar De Potter, Tom. *Functional Imaging and Modelling of the Heart*, volume 10263 of *Lecture Notes in Computer Science*. Springer International Publishing, Cham, 2017.
24. Tomohiro Otani, Abdullah Al-Issa, Amir Pourmorteza, Elliot McEigh, Shigeo Wada, and Hiroshi Ashikaga. A Computational Framework for Personalized Blood Flow Analysis in the Human Left Atrium. *Annals of biomedical engineering*, 44(11):3284–3294, 2016.
25. Catherine M Otto. Heartbeat: Left atrial appendage occlusion for stroke prevention. *Heart*, 103(2):89–90, 2017.
26. Jian Fang Ren, David J. Callans, and Francis E. Marchlinski. What is the natural relationship between left atrial appendage morphology and history of stroke? *Journal of the American College of Cardiology*, 61(6):689–690, 2013.
27. Christian T. Ruff, Robert P. Giugliano, Eugene Braunwald, Elaine B. Hoffman, Naveen Deenadayalu, Michael D. Ezekowitz, A. John Camm, Jeffrey I. Weitz, Basil S. Lewis, Alexander Parkhomenko, Takeshi Yamashita, and Elliott M. Antman. Comparison of the efficacy and safety of new oral anticoagulants with warfarin in patients with atrial fibrillation: a meta-analysis of randomised trials. *The Lancet*, 383(9921):955–962, mar 2014.
28. Filippos Triposkiadis, Burkert Pieske, Javed Butler, John Parissis, Gregory Giamouzis, John Skoularigis, Dirk Brutsaert, and Harisios Boudoulas. Global left atrial failure in heart failure. *European Journal of Heart Failure*, 18(11):1307–1320, 2016.
29. Vijay Vedula, Richard George, Laurent Younes, and Rajat Mittal. Hemodynamics in the left atrium and its effect on ventricular flow patterns. *Journal of Biomechanical Engineering*, 137(November):1–8, sep 2015.
30. Yan Wang, Luigi Di Biase, Rodney p. Horton, Tuan Nguyen, Prasant Morhanty, and Andrea Natale. Left Atrial Appendage Studied by Computed Tomography to Help Planning for Appendage Closure Device Placement. *Journal of Cardiovascular Electrophysiology*, 21(9):973–982, sep 2010.
31. Shadi Yaghi, Yeseon P. Moon, Consuelo Mora-McLaughlin, Joshua Z. Willey, Ken Cheung, Marco R. Di Tullio, Shunichi Homma, Hooman Kamel, Ralph L. Sacco, and Mitchell S.V. Elkind. Left Atrial Enlargement and Stroke Recurrence. *Stroke*, 46(6):1488–1493, 2015.
32. Masayoshi Yamamoto, Yoshihiro Seo, Naoto Kawamatsu, Kimi Sato, Akinori Sugano, Tomoko Machino-Ohtsuka, Ryo Kawamura, Hideki Nakajima, Miyako Igarashi, Yukio Sekiguchi, Tomoko Ishizu, and Kazutaka Aonuma. Complex left atrial appendage morphology and left atrial appendage thrombus formation in patients with atrial fibrillation. *Circulation: Cardiovascular Imaging*, 7(2):337–343, 2014.
33. Lucy T. Zhang and Mickael Gay. Characterizing left atrial appendage functions in sinus rhythm and atrial fibrillation using computational models. *Journal of Biomechanics*, 41(11):2515–2523, aug 2008.

34. Kun Zuo, Lanlan Sun, Xinchun Yang, Xiuzhang Lyu, and Kuibao Li. Correlation between cardiac rhythm, left atrial appendage flow velocity, and CHA2DS2VASc score: Study based on transesophageal echocardiography and 2 dimensional speckle tracking. *Clinical Cardiology*, 40(2):120–125, 2017.